THE JOURNAL OF BIOLOGICAL CHEMISTRY VOL. 289, NO. 46, pp. 32030–32043, November 14, 2014

Global Ablation of the Mouse Rab11a Gene Impairs Early Embryogenesis and Matrix Metalloproteinase Secretion*

Received for publication, May 1, 2014, and in revised form, September 26, 2014 Published, JBC Papers in Press, September 30, 2014, DOI 10.1074/jbc.M113.538223

Shiyan Yu[‡1], Ghassan Yehia[§], Juanfei Wang[¶2], Ewa Stypulkowski[‡], Ryotaro Sakamori[‡], Ping Jiang[‖], Berenice Hernandez-Enriquez[‡], Tracy S. Tran[‡], Edward M. Bonder[‡], Wei Guo[¶], and Nan Gao[‡3]

From the [‡]Department of Biological Sciences, Rutgers University, Newark, New Jersey 07102, the [§]Transgenic Core Facility, Rutgers New Jersey Medical School, Newark, New Jersey 07103, the [¶]Department of Biology, University of Pennsylvania, Philadelphia, Pennsylvania 19104, and the [‖]Cold Spring Harbor Laboratory, Cold Spring Harbor, New York 11724

Background: The physiological role of Rab11a in mouse embryogenesis has not been fully studied.
Results: Using a Rab11a^{null} mouse allele, the transport of multiple membrane-associated and soluble cargos was analyzed in mouse blastocysts and MEFs.
Conclusion: Rab11a ablation impairs mouse blastocyst development and the secretion of soluble matrix metalloproteinases.
Significance: *In vivo* functions of Rab11a in mouse fetal development and soluble MMP secretion were uncovered.

Rab11a has been conceived as a prominent regulatory component of the recycling endosome, which acts as a nexus in the endo- and exocytotic networks. The precise *in vivo* role of Rab11a in mouse embryonic development is unknown. We globally ablated Rab11a and examined the phenotypic and molecular outcomes in Rab11a^{null} blastocysts and mouse embryonic fibroblasts. Using multiple trafficking assays and complementation analyses, we determined, among multiple important membrane-associated and soluble cargos, the critical contribution of Rab11a vesicular traffic to the secretion of multiple soluble MMPs. Rab11a^{null} embryos were able to properly form normal blastocysts but died at peri-implantation stages. Our data suggest that Rab11a critically controls mouse blastocyst development and soluble matrix metalloproteinase secretion.

Precise sorting and trafficking of intracellular proteins is important for host tissue homeostasis. In response to extracellular and intracellular stimulations, a plethora of proteins are *de novo* synthesized in the endoplasmic reticulum (ER),[4] sent to the Golgi complex for modifications, and finally sorted at the trans-Golgi network (TGN) for delivery into distinct cellular compartments for function (1, 2). On the other hand, cell surface receptors are internalized from the plasma membrane via the endocytic pathway. From there, certain membrane-associated receptors, such as the Transferrin receptor (TfR), are sorted and recycled back to the cell surface to be reutilized (3). A pool of molecules, including soluble SNAREs, small GTPases, adaptor proteins, kinases, and cytoskeletal and motor proteins, are directly involved in protein trafficking and/or the regulatory mechanisms (1, 2). Rab superfamily members are key small GTPase regulators that control the processes of vesicular targeting, budding, motility, and fusion (4, 5). The functional impairment of Rab proteins has been associated with many human diseases (4).

Rab11 subfamily members, including Rab11a, Rab11b, and Rab25, are generally considered to regulate the function of a special endosomal subpopulation, the recycling endosome (6). This heterogeneous tubular-vesicular compartment engages in dynamic and intense membrane trafficking, connecting the endo- and exocytotic pathways. Although Rab11a is conceived to be one of the most prominent recycling endosome components, cell culture studies have delineated its roles in broader intracellular domains, encompassing the TGN, post-Golgi secretory vesicles, and the recycling endosome (6, 7). For instance, in addition to recycling activities, Rab11a vesicles have been implicated in the exocytic transport of biosynthetic cargos (8–10). In baby hamster kidney cells, BHK21, overexpression of dominant-negative mutant Rab11aS25N or a GDP dissociation inhibitor selectively inhibited the exit of vesicular stomatitis virus glycoprotein G (VSVG), a biosynthetic cargo, from the Golgi to the plasma membrane (8). In the *Drosophila* egg chamber, Rab11 vesicles transport E-cadherin to the plasma membrane to maintain the junctions between germ cells and niche cap cells (11, 12). A similar finding has been reported in human cervical cancer (HeLa) and canine kidney epithelial (MDCK) cells, suggesting that the Rab11a recycling endosome may be used as an intermediate compartment for the transport of biosynthetic cargos (10). In polarized epithelial cells, Rab11-positive recycling endosomes play a critical role in apical membrane biogenesis (13, 14). Depletion of Rab11a in human colonic epithelial cells (Caco-2) caused the formation of

* This work was supported, in whole or in part, by National Institutes of Health Grants DK085194, DK093809, DK102934, and CA17859 (to N. G.) and Grant GM085146 (to W. G.). This work was also supported by Charles and Johanna Busch Memorial Award 659160 and by Rutgers University Faculty Research Grant 281708 (to N. G.).
[1] Supported by New Jersey Commission on Cancer Research Postdoctoral Fellowship DFHS13PPC016.
[2] Present address: School of Life Sciences, Tsinghua University, Beijing 100084, China.
[3] To whom correspondence should be addressed: Department of Biological Sciences, Rutgers University at Newark, Rm. 206, 195 University Ave., Newark, NJ 07102. Tel.: 973-353-5523; Fax: 973-353-5518; E-mail: ngao@andromeda.rutgers.edu.
[4] The abbreviations used are: ER, endoplasmic reticulum; TGN, trans-Golgi network; TfR, transferrin receptor; VSVG, vesicular stomatitis virus glycoprotein G; MDCK, Madin-Darby canine kidney; MMP, matrix metalloproteinase; MEF, mouse embryonic fibroblast; E6.5, embryonic day 6.5; SEAP, secreted alkaline phosphatase.

multiple lumens under three-dimensional culture conditions (15). Furthermore, viruses such as influenza A virus, Sendai virus, and measles virus hijack Rab11a-positive recycling endosomes to traffic viral progeny ribonucleoprotein complexes to the plasma membrane for viral shedding (16–18). Knockdown of Rab11a causes aberrant perinuclear accumulation of viral ribonucleoprotein complexes, therefore reducing viral release. These studies shed light on the role of Rab11a vesicles in biosynthetic cargo transport.

The precise and timely degradation of the extracellular matrix by secreted MMPs is required for cell migration, embryonic implantation, tissue morphogenesis, and innate immune response (19–21). To fulfill this purpose, MMPs are tightly regulated at multiple levels: transcription, activation of precursor zymogens, and inhibition of the mature enzymes (22). Multiple MMPs, such as MMP2, MMP7, and MMP9, are increasingly detected during mouse blastocyst implantation (23, 24). In contrast to studies of MMPs at expressional or activation levels, the mechanism underlying MMP secretion has not been fully investigated. Emerging studies have started to suggest that the transportation of MMPs might be a key regulatory factor in extracellular matrix remodeling and cancer cell invasion (25). In neurons and macrophages, MMPs are encapsulated into small vesicles associated with motor proteins such as Dynein and Myosin Vb and are transported along microtubules and microfilaments (26, 27). Of note, Myosin Vb is a well characterized binding partner of Rab11a (28). Several SNAREs are also involved in MMP vesicle delivery (29–31). The effect of Rabs on MMP intracellular trafficking and secretion has only been explored recently. In cultured human macrophages, Rab5a, Rab8a, and Rab14 modulate MT1-MMP trafficking for cell migration and invasion (32). In RAW 264.7 cells, Rab3D is required for MMP9 vesicles to associate with Kinesin 5B and to be transported along microtubules (27). In the human breast cancer cell line MDA-MB-231, Rab40b has been shown to mediate MMP2/9 segregation into VAMP4 vesicles and regulate MMP2/9 vesicles trafficking during the formation of invadopodia (33).

Here, using a new Rab11a knockout allele, we explored the functions of Rab11a in mouse embryogenesis. In addition to revisiting a number of previously known Rab11 cargos in this loss-of-function setting, we discovered that Rab11a vesicles critically control the secretion of multiple soluble MMPs. In the absence of Rab11a, the extracellular matrix degradation capacities of both mouse blastocysts and MEFs were weakened. $Rab11a^{null}$ embryos died *in utero* at the implantation stage. Our data established important roles of Rab11a in mouse blastocyst development and soluble MMP secretion.

EXPERIMENTAL PROCEDURES

Derivation of the Mouse $Rab11a^{null}$ Allele—An 11-kb DNA fragment containing the mouse Rab11a genomic locus was retrieved from a bacterial artificial chromosome clone, RP23–21N19, into pL253 using gap repair in EL350 *Escherichia coli* (34). Two loxP sites were then introduced sequentially at 242 bp downstream of the second exon and 210 bp downstream of the fourth exon of Rab11a, respectively (35). The sequence-verified targeting vector was linearized with ClaI digestion and electroporated into R1 embryonic stem cells. Positively targeted clones were screened by Southern blot analyses using ^{32}P-labeled 5′ and 3′ external probes that distinguished wild-type and targeted alleles upon EcoRI and SacI digestion. Blastocyst injections resulted in eight chimeric mice, all of which transmitted the targeted allele through the germ line. An Frt-Neo-Frt cassette was then removed using ACT-FLPe mice (The Jackson Laboratory, catalog no. 003800) (36). The $Rab11a^{null}$ allele was derived by crossing $Rab11a^{fl/+}$ mice to EIIa-Cre mice (The Jackson Laboratory, catalog no. 003314) (37). To inducibly delete Rab11a in post-implantation embryos, Rosa26-CreER mice (Jackson Lab, catalog no. 008463) (38) were used to derive $Rab11a^{fl/fl}$;Rosa26-CreER mice. $Rab11a^{fl/fl}$ females plugged by $Rab11a^{fl/fl}$;Rosa26-CreER males were gavaged with corn oil-dissolved tamoxifen to ablate Rab11a at E6.5 and E8.5. Embryos were then collected and genotyped after a few days of tamoxifen feeding. Mouse experimental procedures were approved by the Rutgers Institutional Animal Care and Use Committees.

Plasmids—pmCherry-VSVG was constructed by subcloning VSVG-encoding sequences in-frame into the pmCherry-N1 vector. pmEGFP was generated by inserting oligonucleotides encoding the first 10 amino acids (MGCVCSSNPE) of mouse Lck into XhoI/EcoRI sites of the pEGFP N1 vector to fuse the plasma membrane-targeting motif (39) to enhanced green fluorescent protein at its N terminus. Human TGN38-encoding sequences were cloned in-frame into the pmCherry-N1 vector to generate a C-terminal mCherry-tagged TGN38 plasmid, pTGN38-mCherry. pmCherry-RAB11A was generated by sequentially inserting mCherry and human RAB11A coding sequences into the pQCXIP retroviral vector to create N-terminal mCherry-tagged RAB11A. pEGFP-KDEL was provided by Dr. Nihal Altan-Bonnet (NHLBI, National Institutes of Health). The pSEAP vector encoding a heat-stable secreted human placental alkaline phosphatase driven by the SV40 promoter and pRL-TK were purchased from Clontech and Promega, respectively.

Fertilized Egg Isolation, Culture, and Outgrowth—Superovulated heterozygous females were caged overnight with heterozygous males and checked for the presence of copulation plugs early the next morning. Plugged females were euthanized to dissect out the ovaries and oviducts. Under an inverted microscope, the ampulla was torn, and embryos were released into a hyaluronidase/M2 solution (Millipore, catalog nos. 389561–100U and MR-015-D) for dissociation of cumulus cells. After washing briefly, embryos were transferred and cultured under oil in drops of M16 medium (Millipore, catalog no. MR-010-D) for the indicated days.

MEF Isolation, Culture, and Cre Transduction—E12.5 $Rab11a^{fl/fl}$ embryos were removed from the uterus. The trunk was minced by sterile scissors and digested with 1× trypsin/EDTA at 37 °C for 30 min. Tissue chunks were pipetted up and down to dissociate the cells. After centrifugation at 200 × *g* for 2 min, the cell suspension was seeded into DMEM containing 10% fetal bovine serum and penicillin/streptomycin solution. For Cre transduction, MEF cells were exposed to CMV promoter-driven Cre retroviruses for 3 h and selected by 500 μg/ml hygromycin B for 3 weeks. Rab11a-deficient MEF cells ($Rab11a^{null}$) were maintained with normal DMEM containing

100 μg/ml hygromycin B. Rab11a^{null} MEFs rescued by human Rab11A were established by infection of the cells with retroviral mCherrry-tagged full-length human RAB11A (nCherry-RAB11A) and stable selection with 3 μg/ml puromycin.

Genomic PCR—Genomic DNA was prepared from individual mice or embryos in a buffer containing 10 mM Tris-HCl (pH 8.3), 50 mM KCl, 2 mM $MgCl_2$, 0.1 mg/ml gelatin, 0.45% Nonidet P-40, 0.45% Tween 20, and 100 μg/ml of proteinase K at 55 °C overnight. Proteinase K was then deactivated at 95 °C for 10 min, and the supernatant was used for PCR reactions. Genotyping PCR was performed by using primer sets specific for Rab11a wild-type (400 bp) and loxP alleles (564 bp, forward, 5′-CCAAGACCTTC-CTTCAATGCCTACA (P1); reverse, 5′-ATGCTGGAAAGA-TGGCTCAGCAGTT (P2)) and the Rab11a^{null} allele (forward P1 and reverse, TGTGAGCCACCCCGCATGGGTGCTG (P3)).

Transferrin Uptake and Recycling Assay—5×10^4 MEF cells were seeded into 4-well chamber slides and incubated overnight. Before incubation with Alexa Fluor 568-conjugated transferrin (Life Technologies, catalog no. T23365), cells were placed on ice for 10 min, washed three times with cold live cell imaging solution (Life Technologies, catalog no. A14291DJ), and incubated with prewarmed live cell imaging solution containing 25 μg/ml transferrin 568, 20 mM glucose, and 1% BSA at 37 °C. For the uptake assay, cells were trypsinized, fixed at the indicated time point, and subjected to flow cytometric analysis. For recycling assay, cells were washed three times with cold live cell imaging solution after 30 min incubation and chased for fluorescence intensity in warmed live cell imaging solution (250 μg/ml unlabeled transferrin, 20 mM glucose, and 1% BSA) for the indicated time.

Matrix Degradation Assay—To evaluate the matrix degradation capacity of Rab11a$^{-/-}$ blastocysts *in vitro*, hatched blastocysts (genotype as Rab11a$^{+/+}$, Rab11a$^{+/-}$, and Rab11a$^{-/-}$, respectively) collected from Rab11a$^{+/-}$ plug-mating were transferred in to a gelatin 568/collagen I-coated coverslip for outgrowth. After 2–3 days in culture, blastocysts were fixed with 10% neutral formalin and stained for Rab11a to identify null blastocysts from controls (including wild-type and heterozygotes). Alexa Fluor 350 phalloidin (Life Technologies, catalog no. A22281) was used to outline embryo edges. To assess the matrix degrading ability of MEFs, 5×10^4 MEFs were seeded on the mixed matrix (Alexa Fluor 568 gelatin and collagen I fibrils) coated coverslips and incubated for 2 days for degradation at 37 °C. Cells were fixed and processed for immunofluorescence.

Gelatin degradation was quantified using NIH ImageJ software and reported as the total area of degradation zones per cell relative to the area of the whole cell. Quantification was done in three independent experiments.

In-gel Zymography Assay—The in-gel gelatin zymography assay was performed as described previously (40). 2×10^5 MEF cells were seeded in each well of a 6-well plate. Opti-MEM was used for starvation for 24 h after confluence. The culture media were collected and concentrated by filtration using Microcon concentrators (Millipore, catalog no. MRCPRT010), and the cells were lysed for Western blot analyses. Samples were mixed with SDS loading buffer (10% SDS, 50% glycerol, 0.4 M Tris (pH 6.8), and 0.1% bromphenol blue) and separated on 8% polyacrylamide/0.3% gelatin gels. After electrophoresis, the gels were washed twice in 2.5% Triton X-100 for 1 h and then incubated in reaction buffer (50 mM Tris (pH 8.0) and 5 mM $CaCl_2$) at 37 °C for 6 h before being stained with Coomassie Blue R-250.

MMP7 Kinetics Assay—Fertilized eggs were harvested and cultured individually in equal volumes of M16 medium (FBS-free) and covered with oil until hatching. Equivalent volumes (a total of 6 μl) of culture medium were collected and used for the MMP7 activity assay, and the embryos were genotyped after the assay. MMP7 enzyme kinetics were analyzed using the SensoLyte 520 MMP-7 assay kit (AnaSpec, catalog no.71153) according to the recommendations of the manufacturer. Briefly, MMP7 was activated via incubation with culture medium with 1 mM 4-aminophenylmercuric acetate (APMA) for 1 h at 37 °C. An equal volume of MMP7 substrate-containing solution was added to the medium and mixed gently for 30 s. Blank M16 medium and MMP7-containing FBS were used as negative and positive controls, respectively. The fluorescence intensity derived from 5-FAM upon MMP7-catalyzed cleavage was measured immediately at 490/520 nm (excitation/emission) and recorded continuously for 90 cycles using the GloMax-Multi detection system (Promega).

Secreted Alkaline Phosphatase (SEAP) Activity Assay—1×10^5 MEFs were seeded into a 12-well plate. After overnight growth, cells were cotransfected with the pSEAP and pRL-TK vectors using Lipofectamine 3000 (Life Technologies, catalog no. L3000-015) according to the instructions of the manufacturer. Cell culture media were harvested for centrifugation at 12,000 $\times$ *g*, heat-inactivated at 65 °C to eliminate endogenous alkaline phosphatase activity, and then subjected to heat-resistant truncated alkaline phosphatase activity assay according to the manual of the manufacturer. For measuring intracellular SEAP activity, cell lysates were prepared with passive lysis buffer (Promega), denatured at 65 °C, and subjected to activity measurements. The transfection efficiency was normalized by *Renilla* luciferase activities.

MMP2 ELISA—3×10^5 MEF cells were seeded into each well of a 6-well plate. After 12 h, culture media were replaced by 1.5 ml of fresh DMEM in the presence or absence of 10 μM monensin (Sigma, catalog no. M5273). Cells were harvested after 12 h of incubation. Culture media were centrifuged at 3,000 $\times$ *g* for 10 min, and 100 μl of supernatant was subjected to mouse MMP2 ELISA (Abcam, catalog no. ab100730) according to the manual of the manufacturer.

RT-PCR—Total RNAs were extracted from embryos at the four-cell, morula, and blastocyst stages using TRIzol (Life Technologies, catalog no. 15596-018). Complementary DNAs were synthesized by reverse transcriptase according to the instructions of the manufacturer (Thermo Fisher). Specific primers used in PCR reactions were as follows: Rab11a, 5′-CATGCTT-GTGGGCAATAAGA-3′ (forward) and 5′-TTGGCTTGTTCT-CAGTGTG-3′ (reverse); Rab11b, 5′-TGCTTATTGGGGACT-CAGGT-3′ (forward) and 5′-CCACCAGCATGATGACAATG-3′ (reverse); and β-actin, 5′-TTCTTTGCAGCTCCTTCGTT-3′ (forward) and 5′-CTTCTCCATGTCGTCCCAGT-3′ (reverse).

Confocal Immunofluorescence—The procedure of confocal immunofluorescence has been described previously (41). Briefly, 1×10^3 MEF cells were seeded onto chamber slides or a

live cell imaging chamber. Cells were transfected with the indicated plasmids. After 12 h, cells were checked for epifluorescence or fixed with 4% paraformaldehyde at room temperature for 20 min and then subjected to indirect immunofluorescence. Blastocysts were fixed in cold 4% paraformaldehyde in PBS at room temperature for 30 min and permeabilized with 1% Triton X-100 in PBS for 10 min. After blocking in 5% donkey serum and 5% bovine serum albumin in PBS for 2 h, blastocysts were incubated with primary antibodies diluted in blocking buffer overnight at 4 °C. The next morning, blastocysts were washed with PBS for 30 min at room temperature and incubated with fluorescently conjugated secondary antibodies and TOPRO-3 (1:1000, Life Technologies, catalog no. T3605) for 2 h. After intensive washes, embryos were mounted in microdrops on a glass cover and analyzed by a Zeiss 510 laser-scanning confocal microscope.

The antibodies used were as follows: mouse anti-Rab11a (1:200, BD Transduction Laboratories; catalog no. 610656), rabbit anti-Rab11a (1:200, US Biological, catalog no. R0009), mouse anti-Cdx2 (1:100, Biogenex, catalog no. CDX2-88), goat anti-MMP7 (1:200, Santa Cruz Biotechnology; catalog no. sc-8832), mouse anti-E-cadherin (1:200, BD Transduction Laboratories, catalog no. 610181), rabbit anti-MMP2 (1:200, Santa Cruz Biotechnology; catalog no. sc-10736), rat anti-LAMP2 (1:200, DHSB, catalog no. ABL-93), goat anti-GFP (1:500, Abcam, catalog no. ab6673), and rat anti-GRP94 (1:250, Abcam, catalog no. ab2791).

RESULTS

Rab11a Ablation Caused Embryonic Lethality—To determine Rab11a function in mice, we first derived a conditional mouse Rab11a allele by homologous recombination in embryonic stem cells. Two loxP sites were introduced to flank the third and fourth exons of the Rab11a gene at chromosome 9 (Fig. 1*A*). Positively targeted stem cell clones were verified by Southern blot analyses and used to generate chimeric mice (Fig. 1*B*). The desired loxP allele was transmitted through the germ line (Fig. 1*C*).

To generate $Rab11a^{null}$ mice, we crossed Rab11a loxP ($Rab11a^{fl/fl}$) mice with EIIa-Cre transgenic mice that facilitate gene deletion at zygotic stages (37). The resulting $Rab11a^{\Delta Exon3-4}$ allele from Cre-mediated recombination was detected by genomic PCR with primers flanking two loxP sites (Fig. 1*A*, primers *P1* and *P3*). This $Rab11a^{\Delta Exon3-4}$ allele is likely a null allele because the targeted two exons encode the small GTPase domain of Rab11a (Fig. 1*A*). The deletion also introduced a frameshift and disrupted the downstream coding sequence. We then crossed $Rab11a^{+/-}$; EIIa-Cre mice with wild-type mice and transmitted the $Rab11a^{null}$ allele through the germ line. The resulting $Rab11a^{+/-}$ mice without the EIIa-Cre transgene were intercrossed to produce homozygous knockouts ($Rab11a^{-/-}$) along with wild-type ($Rab11a^{+/+}$) and heterozygous ($Rab11a^{+/-}$) littermates.

Using PCR primers designed to specifically amplify the null and wild-type alleles, we genotyped 166 live pups from over 10 different heterozygous mating pairs and did not detect a single $Rab11a^{-/-}$ pup (Fig. 1*D*). We then analyzed embryos from E7.5 to E15.5 stages following plug-mating of $Rab11a^{+/-}$ mice. Again, no $Rab11a^{null}$ embryo was detected from these stages (Fig. 1*D*). The ratios between $Rab11a^{+/+}$ and $Rab11a^{+/-}$ mice at both newborn and E7.5–15.5 stages were close to 1:2, as anticipated from Mendel's laws (Fig. 1*D*). We examined uterus sections from superovulated $Rab11a^{+/-}$ females at 5–6.5 days post-coitum and immunostained for Rab11a (Fig. 1*E*). All implanted embryos stained positively for Rab11a (Fig. 1*E*, *bottom panel*), suggesting that null embryos were likely growth-arrested at an earlier fetal stage.

To gain some insights into which developmental stage(s) was/were impaired by Rab11a deletion, we isolated fertilized eggs and monitored their embryogenesis in culture (Fig. 1, *F* and *G*). We genotyped 112 embryos that showed hatching morphologies after 4–5 days of culture and observed that $Rab11^{-/-}$ blastocysts were, in fact, capable of developing into blastocysts *in vitro*, and, remarkably, some even proceeded into the hatching stage (Fig. 1, *G* and *H*). The hatching capability of blastocysts in the presence and absence of Rab11a after 4 days in culture was $Rab11a^{+/+}$ (33.3%), $Rab11a^{+/-}$ (35.6%), and $Rab11a^{-/-}$ (40%) (Fig. 1*I*), suggesting that loss of Rab11a did not prevent the embryo from forming blastocysts and hatching.

To determine whether $Rab11a^{null}$ embryos died during the implantation stages, we employed an inducible Rab11a deletion strategy using Rosa26-CreER mice, which globally ablate gene targets in a tamoxifen-inducible fashion (38). We crossed $Rab11a^{fl/fl}$;Rosa26-CreER males with $Rab11a^{fl/fl}$ females, and, by delivering tamoxifen to the pregnant females, we induced Rab11a ablation in E6.5 or E8.5 embryos that had completed implantation stages. If Rab11a deletion at these stages was lethal to the embryos, we would anticipate that no Rab11a-deficient embryos would be recovered. Otherwise, 50% of embryos should carry the CreER gene, therefore showing the $Rab11a^{null}$ allele. Remarkably, we detected the $Rab11a^{null}$ allele in ~50% of embryos, which were induced for deletion at E6.5 or E8.5 (Fig. 1*J*). In addition, inducible Rab11a-deficient embryos recovered at E10.5 showed beating hearts, indicating viability (data not shown). Together, despite the potential submaximal deletion of Rab11a by Rosa26-CreER in embryos, these inducible Rab11a deletion results suggested that loss of Rab11a might have impacted the implanting blastocysts.

Impaired Cargo Trafficking in $Rab11a^{null}$ MEFs—Early embryonic lethality caused by global Rab11a deletion impeded our direct analysis of affected cargo trafficking in $Rab11a^{null}$ embryos. To circumvent this obstacle, we derived $Rab11a^{null}$ MEFs using Cre-expressing retroviruses. Stable $Rab11a^{null}$ MEF clones were established by antibiotic selection. Western blot analysis for Rab11a confirmed an efficient deletion of Rab11a in the stable $Rab11a^{fl/fl}$; Cre^{+} MEFs compared with control $Rab11a^{fl/fl}$ MEFs without Cre viral infection (Fig. 2*A*).

Previous studies have demonstrated that ligand-bound transferrin receptors, upon endocytosis, are returned to the cell surface through recycling endosomes (42, 43). Using transferrin recycling assays, we indeed observed a markedly reduced recycling of transferrin in $Rab11a^{null}$ MEFs compared with wild-type MEFs (Fig. 2, *B* and *C*). This observation was consistent with the inhibitory effect elicited by the Rab11a dominant-negative S25N mutant (42, 43). The residual recycling activity observed in $Rab11a^{null}$ MEFs might be mediated by other recy-

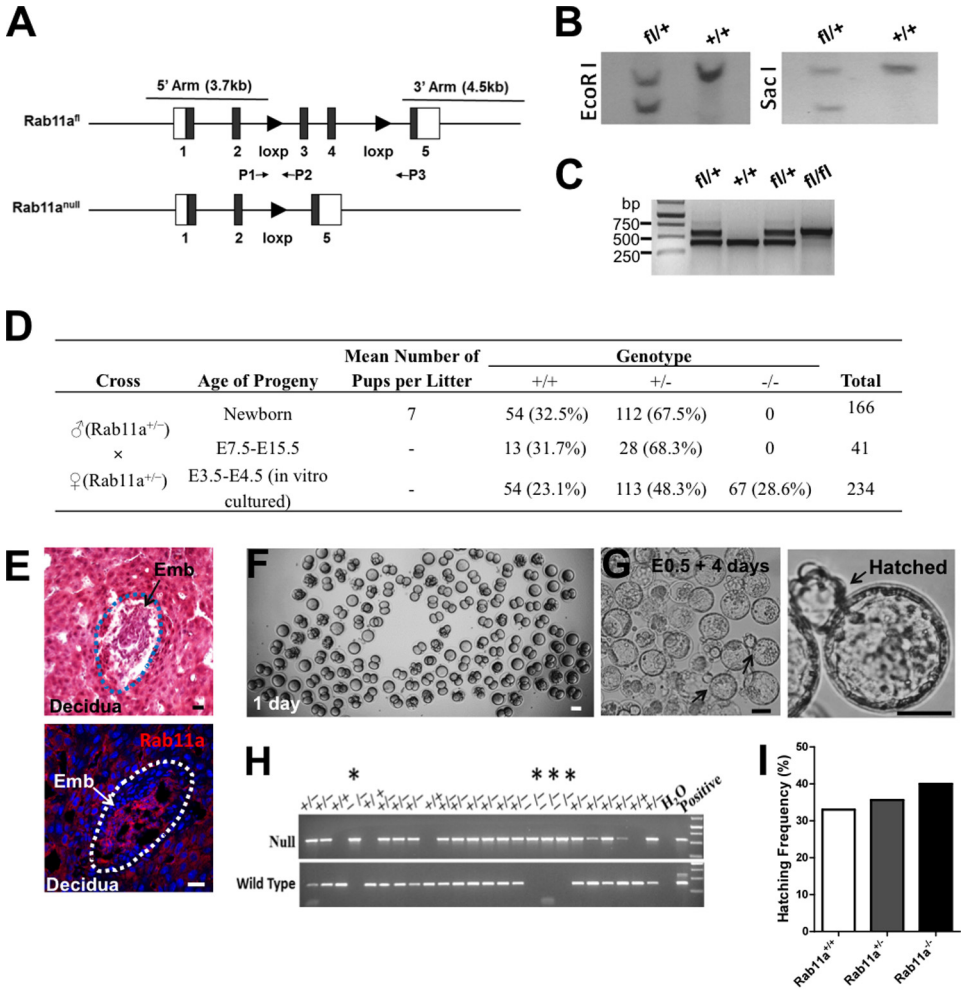

Cross	Age of Progeny	Mean Number of Pups per Litter	Genotype +/+	Genotype +/-	Genotype -/-	Total
♂(Rab11a$^{+/-}$) × ♀(Rab11a$^{+/-}$)	Newborn	7	54 (32.5%)	112 (67.5%)	0	166
	E7.5-E15.5	-	13 (31.7%)	28 (68.3%)	0	41
	E3.5-E4.5 (in vitro cultured)	-	54 (23.1%)	113 (48.3%)	67 (28.6%)	234

J

Cross	Tamoxifen Feeding at	Genotyped at	Detection of Rab11a^{null} Allele	Total
♂ (Rab11a$^{fl/fl}$; Rosa26-CreER) × ♀ (Rab11a$^{fl/fl}$)	E6.5	E8.5	12 (48%)	25
	E6.5	E9.5	4 (36.4%)	11
	E8.5	E10.5	4 (50%)	8
	E8.5	Newborn	5 (31.3%)	16

FIGURE 1. **Rab11a global knockout mice die at the peri-implantation stage.** *A*, schematics of Rab11a^{flox} and Rab11a^{null} alleles. *P1*, *P2*, and *P3* represent genomic PCR primers to identify specific alleles. *B*, Southern blots confirmed correctly targeted ES cell clones. *C*, PCR using the primer set P1 and P2 confirmed the derivation of Rab11a$^{fl/fl}$ mice. *D*, summary of genotyping results of 166 neonatal pups and 275 embryos produced from intercrossing Rab11a$^{+/-}$ mice. 67 live Rab11a^{null} embryos were identified from *in vitro* cultured blastocysts. No live null embryos or pups were detected *in utero* or after birth. *E*, representative implanted embryos (*Emb*), all of which were Rab11a-positive wild types. H&E and Rab11a staining of uterus sections is shown. *Scale bars* = 10 μm. *F*, fertilized eggs (E0.5) from Rab11a$^{+/-}$ mating were cultured for 1 day *in vitro*. *Scale bar* = 50 μm. *G*, after 4 days of development in culture, Rab11a^{null} blastocysts underwent hatching (*arrows*). *Scale bars* = 40 μm. *H*, genotyping of individual hatched blastocysts identified Rab11a^{null} embryos (*asterisks*). *I*, Rab11a^{null} embryos demonstrated equivalent hatching activity as wild types. *J*, Rab11a was inducibly deleted from E6.5 or E8.5 embryos via tamoxifen-gavaging pregnant Rab11a$^{fl/fl}$ females, which were plugged by Rab11a$^{fl/fl}$;Rosa26-CreER males. A summary of the genotyping results showed the positive detection of null alleles from live embryos collected at the designated time points.

cling regulators, such as Rab4 (42, 43). Of note, we did not detect a significant reduction or delay of transferrin uptake by Rab11a^{null} MEFs (Fig. 2*C*). Furthermore, after 3 h, ~74% of transferrins were recycled, even in Rab11a^{null} MEFs (Fig. 2*B*). Collectively, these results suggested that Rab11a deletion significantly reduced the efficiency of TfR recycling but did not completely block the process.

Given that another critical role of recycling endosome is the export of biosynthetic cargos (2, 44), we examined whether the cell surface delivery of the well characterized VSVG was affected after genetic ablation of Rab11a. Wild-type as well as Rab11a^{null} MEFs were cotransfected with mCherry-VSVG with a plasma membrane-targeted enhanced GFP (mEGFP). Cells were subjected to confocal fluorescent analysis after 12 h of transfection. As shown in Fig. 2*D*, newly synthesized VSVG in control MEFs was targeted onto a plasma membrane highlighted by membrane-bound EGFP. Similar observations were made in Rab11a^{null} MEFs, with no clear reduction of membrane-targeted VSVG being detected in Rab11a^{null} MEFs (Fig. 2*D*, *bottom row*). At this point, we were unable to formally prove whether there was a reduction in the speed or efficiency of the plasma membrane targeting of VSVG vesi-

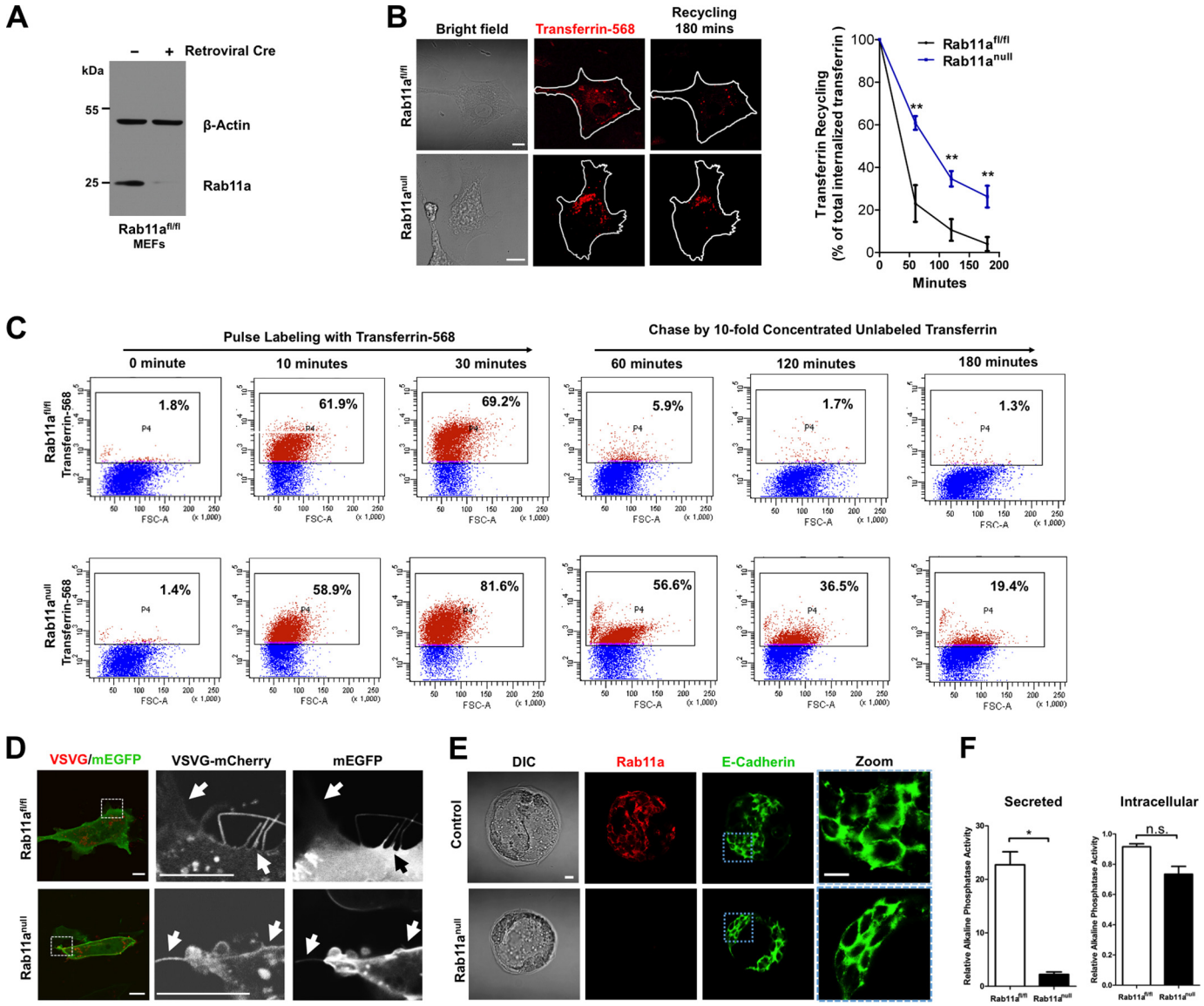

FIGURE 2. **Rab11a deletion affects recycling and export of selected cargos.** *A*, Western blots showed the deletion of Rab11a from retroviral Cre-infected stable Rab11a$^{fl/fl}$ MEFs. Rab11a^{null} MEFs were established after retroviral Cre infection and antibiotic selection (see "Experimental Procedures"). *B*, transferrin recycling assays using live cell confocal fluorescent microscopy. Increased intracellular transferring retention following endocytosis was detected in Rab11a^{null} MEFs, suggesting reduced TfR recycling in these cells compared with wild-type cells. **, $p < 0.01$. Data represent three independent experiments. *Scale bars* = 10 μm. *C*, flow cytometric analyses of wild-type and Rab11a^{null} MEFs that were pulse-treated with transferrin 568 to determine endocytosis and chased with non-labeled transferrin to access recycling activity. Rab11a^{null} MEFs showed reduced recycling activity compared with wild types. *FSC-A*, forward scatter area. *D*, live cell fluorescent analyses of wild-type and Rab11a^{null} MEFs cotransfected with VSVG-mCherry and plasma membrane-targeted enhanced GFP (*mEGFP*) that labels the cell surface. Cells were imaged 12 h after transfection. *Arrows* point to cell surface VSVG. *E*, immunofluorescent analysis of Rab11a (*red*) and E-cadherin (*green*) in wild-type and Rab11a^{null} blastocysts developed *in vitro*. Note that E-cadherin localized to intercellular junctions in Rab11a^{null} blastocysts. *Scale bars* = 10 μm. *DIC*, differential interference contrast. *F*, chemiluminescent analysis of the secretion of a heat-resistant alkaline phosphatase (SEAP). Alkaline phosphatase activities in MEF culture media (*secreted*, *left panel*) and MEF lysates (*intracellular*, *right panel*) were normalized to *Renilla* luciferase activities. *, $p < 0.05$; *n.s.*, not significant.

cles in Rab11a^{null} MEFs. However, just as the ultimate recycling of TfR occurred in Rab11a^{null} MEFs (Fig. 2*B*), the plasma membrane localization of VSVG, a membrane-associated biosynthetic cargo, did not appear to be drastically perturbed in absence of Rab11a. These data were in accordance with the notion that transmembrane biosynthetic cargos such as VSVG may be delivered to the plasma membrane via alternative routes, such as the adaptor protein 3 and 4-dependent pathway (45, 46).

Previous studies have reported that Rab11a traffics E-cadherin (10, 11, 47), which plays a critical role during embryonic compaction (48, 49). We speculated that mislocalization of E-cadherin in Rab11a^{null} blastocysts might explain their early embryonic lethality. However, when we examined E-cadherin localization in Rab11a^{null} blastocysts by costaining E-cadherin and Rab11a, we did not observe significant difference in E-cadherin membrane location between wild-type and Rab11a^{null} blastocysts (Fig. 2*E*). Indeed, the normal localization of E-cadherin in Rab11a^{null} embryos was consistent with the fact that these embryos properly formed blastocysts, as any abnormal E-cadherin trafficking would impede the formation of a polarized blastocyst at this developmental stage (48, 49). These

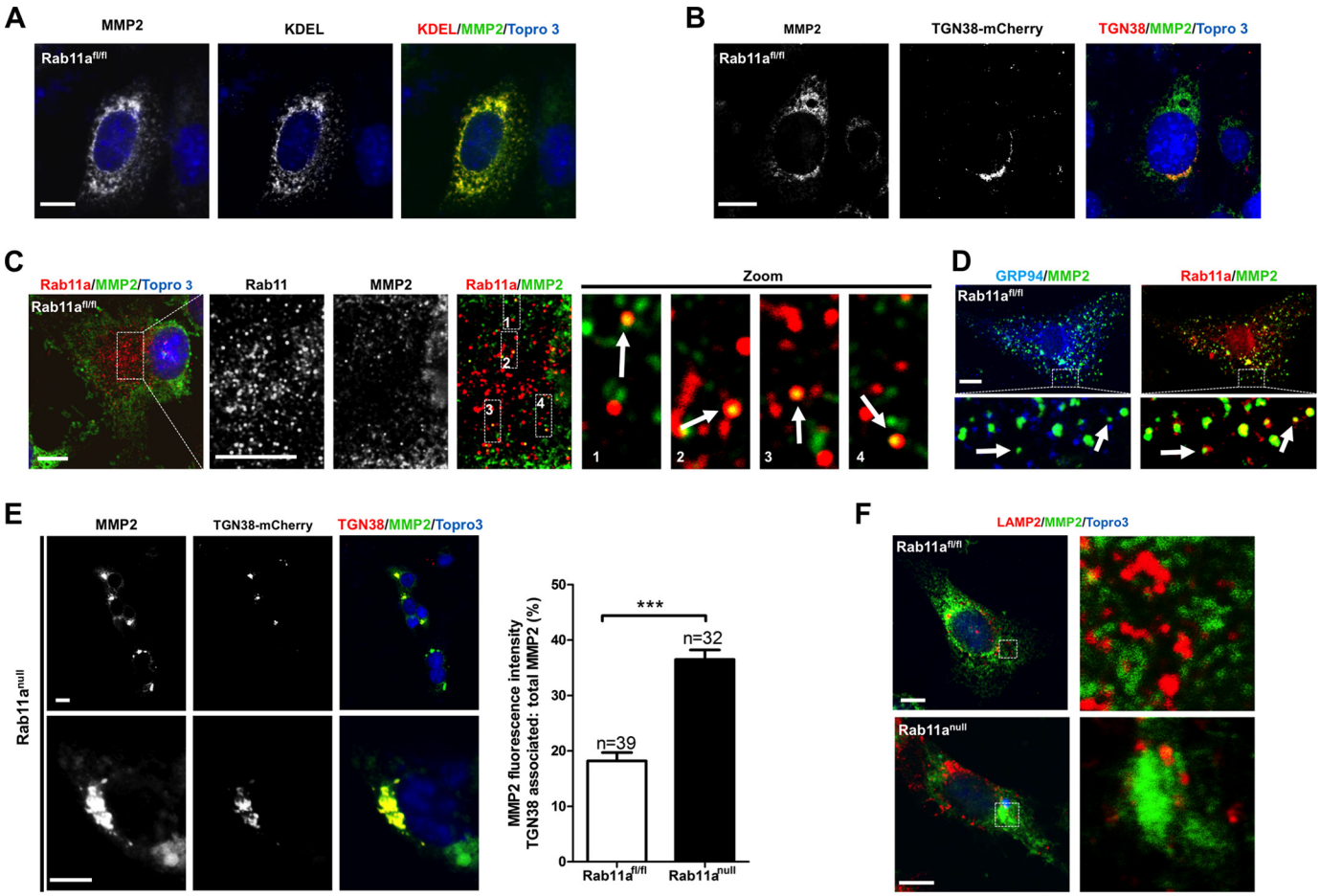

FIGURE 3. **Rab11a vesicles intersect MMP2 vesicular export.** *A* and *B*, confocal immunofluorescent staining of wild-type MEFs for endogenous MMP2 (*green*) showed that the large majority of MMP2 was in the ER (*red*, *A*, *KDEL*), whereas a small portion of MMP2 (*green*) was localized in the TGN (*red*, *B*, *TGN38-mCherry*). *Scale bars* = 10 μm. KDEL-EGFP was pseudocolored as *red*. *KDEL*, ER retention motif with amino acid sequence as lysine-aspartic acid-glutamic acid-leucine. *C*, confocal immunofluorescent staining of wild-type MEFs for endogenous MMP2 (*green*) and Rab11a (*red*) showed that a small fraction of MMP2$^+$ vesicles were positive for Rab11a. *Scale bars* = 10 μm. *D*, confocal immunofluorescent staining of wild-type MEFs for endogenous GRP94 (*blue*), MMP2 (*green*), and Rab11a (*red*) showed Rab11a-positive, ER-negative MMP2 vesicles. *Scale bar* = 10 μm. *E*, confocal immunofluorescent staining of Rab11a^{null} MEFs for endogenous MMP2 (*green*) and TGN (*red*, *TGN38-mCherry*) showed a clear aggregation of MMP2 in the TGN. Note that all Rab11a^{null} MEF cells displayed an identical MMP2 aggregation pattern regardless of whether or not they received a TGN38-mCherry transfection. Untransfected cells are indicated by *arrows*. The *bar graph* shows the percentages of TGN-associated MMP2 in wild-type *versus* Rab11a^{null} MEFs. ***, $p < 0.001$. *Scale bars* = 10 μm. *F*, confocal immunofluorescent staining of wild-type and Rab11a^{null} MEFs for endogenous MMP2 (*green*) and LAMP2 (*red*). No colocalization was detected in either cell type. *Scale bars* = 10 μm.

results suggested that Rab11a is dispensable for E-cadherin trafficking at least in mouse blastocysts.

We then examined whether Rab11a deletion impacted soluble cargo delivery in MEFs. We cotransfected wild-type and Rab11a^{null} MEFs with a heat-resistant secreted placental alkaline phosphatase (50) and *Renilla* luciferase. After 12 h of transfection, cell culture medium and cell lysates were harvested for chemiluminescence analysis. Of note, we detected a significant reduction of alkaline phosphatase activity in media from Rab11a^{null} MEF cultures compared with those from wild-type MEF cultures (Fig. 2*F*). In contrast, there was no significant difference of intracellular alkaline phosphatase activity between control MEFs and Rab11a^{null} MEFs (Fig. 2*F*). These results indicated that secretion of alkaline phosphatase, an artificial soluble cargo, was affected by the absence of Rab11a.

Impaired MMP2 Secretion by Rab11a-deficient MEFs—The embryonic lethality of Rab11a knockout mice strongly implied the potential involvement of Rab11a in the peri-implantation stage. During this short period, mouse embryos undergo stupendous morphological changes and secrete a series of hormones, cytokines, and proteinases to communicate with the uterus to create a favorable implantation environment (51, 52). Given the critical roles of Rab11a in exocytic pathways, secreted cargos that contribute to fetal uterine interaction might potentially be affected in absence of Rab11a. During fetal implantation, trophoblasts secrete MMPs at the implantation site to degrade the uterine wall, and *in vitro* studies suggest that this process is essential for successful implantation and placentation (51). Prompted by the above observation that secretion of a soluble cargo SEAP was reduced dramatically in Rab11a^{null} MEFs, and, according to recent reports on Rab40b-mediated MMP2/9 transport (33), we explored the potential impact of Rab11a deletion on MMP secretion.

We first used wild-type MEFs and detected MMP2 subcellular distribution with confocal immunofluorescence. Consistent with MMP2 being a biosynthetic cargo, the majority of endogenous MMP2 protein (80 ± 3%) was localized in the ER (Fig. 3*A*, *KDEL*), with a relatively small portion localized in the TGN

(Fig. 3*B*, *TGN38-mCherry*) and post-Golgi vesicles (see below). When we costained for endogenous Rab11a and MMP2 in wild-type MEFs, we detected a small fraction of $MMP2^+$ vesicles positive for Rab11a (Fig. 3*C*). To estimate the approximate proportion of non-ER MMP2 vesicles that were positive for Rab11a, we examined wild-type MEFs costained with an ER resident protein, GRP94, MMP2, and Rab11a (Fig. 3*D*). Approximately 14.8 ± 5% of non-ER MMP2 vesicles were $Rab11a^+$, as calculated from 10 random fields. These results implied that a small portion of newly synthesized MMP2 entered the secretory pathway, which was in contrast to our anticipation that MMP2 is being exported constitutively as vesicular cargo. Strikingly, in $Rab11a^{null}$ MEFs, we consistently observed a significant accumulation of MMP2 in the Golgi compartment, identified by TGN38-mCherry (Fig. 3*E*). These MMP2-containing subcellular organelles appeared as large tubular puncta. To rule out mistrafficking of MMP2 into endolysosomal compartments, we performed costaining for MMP2 and the lysosomal marker LAMP2. MMP2 was not accumulated in $LAMP2^+$ compartments of wild-type or $Rab11a^{null}$ MEFs (Fig. 3*F*). These results suggested that MMP2 exocytic transport might be blocked at the TGN in the absence of Rab11a vesicles.

To evaluate, from a functional perspective, whether there was a defect in MMP secretion by $Rab11a^{null}$ MEFs, we performed extracellular matrix degradation assays. $Rab11a^{null}$ and wild-type MEFs were seeded onto coverglasses coated with fluorescent moiety-tagged gelatin (red) and allowed to grow for 5 days. Cells were then fixed, costained with phalloidin 488, and subjected to fluorescent imaging. In contrast to wild-type MEFs, $Rab11a^{null}$ MEFs showed significantly reduced degradation activity on the extracellular matrix (Fig. 4*A*), suggesting that less gelatinases (MMP2/9) were secreted by $Rab11a^{null}$ MEFs.

We quantified secreted MMPs in the conditioned culture media from wild-type and $Rab11a^{null}$ MEFs using in-gel gelatin zymography. Compared with wild-type MEFs, significant reductions (25-fold for MMP2 and 5-fold for MMP9) in gelatin degradation by $Rab11a^{null}$ MEF conditioned media were observed (Fig. 4*B*). This marked reduction of gelatin degradation supported the notion that $Rab11a^{null}$ MEFs secreted less MMP2. The relative stable intracellular MMP2 protein levels in $Rab11a^{null}$ MEFs again indicated that only a small proportion of the enzymes were secreted (Fig. 4*B*). Alternatively, null cells might adapt to the secretory defect by modulating MMP2 production at a transcriptional level (22).

To test whether the observed reduction of MMP2 and MMP9 secretion was caused directly by Rab11a deficiency in the MEFs, we infected $Rab11a^{null}$ MEFs with a lentiviral human RAB11A tagged with an N-terminal mCherry. Expression of this fusion mCherry-RAB11A was confirmed by Western blot analysis in stably selected mCherry-RAB11A MEFs (Fig. 4*C*). Notably, confocal analyses detected positive colocalizations between the endogenous $MMP2^+$ vesicles and the exogenous mCherry-RAB11A in these "rescued" MEFs (Fig. 4*D*). Of note, in-gel gelatin zymography (Fig. 4*E*) and MMP2-specific ELISA (Fig. 4*F*) detected a partial restoration of MMP2 secretion in these rescued MEFs. The failure to fully restore MMP2 secretion in $Rab11a^{null}$ MEFs might be attributed to the potential non-equivalent functions of endogenous mouse Rab11a and the tagged human counterpart. Alternatively, low expression levels of exogenous mCherry-RAB11A and/or the potential steric hindrance by the tag might also account for the observed partial rescue.

Interestingly, compared with wild-type MEFs, $Rab11a^{null}$ MEFs reduced MMP2 secretion by 77.6% (Fig 4*F*). This effect resembled wild-type MEFs treated by monensin, an inhibitor of the recycling trafficking (53, 54). Furthermore, the partially restored MMP2 secretion in rescued $Rab11a^{null}$ MEFs was sensitive to the blockage by monensin (Fig. 4*F*). Taken together, these data strongly support the notion that MMP2 secretion in MEFs is sensitively influenced by Rab11a function.

Impaired MMP7 Secretion in $Rab11a^{null}$ Mouse Blastocysts—During the course of implantation, blastocysts secret several MMPs to facilitate embryo invasion into the maternal uterus (24, 55, 56). Given the critical involvement of MMPs in such fetal uterus interaction, we explored the potential impact of Rab11a deletion on MMP secretion in mouse blastocyst.

Using RT-PCR, we first verified the expression of Rab11a and Rab11b in mouse embryos from the four-cell stage and onward (Fig. 5A). Confocal immunofluorescent analysis detected perinuclear localization of Rab11a in blastocysts, including both the inner cells and the $Cdx2^+$ trophectoderm cells (Fig. 5B).

When we costained wild-type blastocysts for Rab11a and MMP7 (Fig. 5*C*), we found a clear association or overlapping of $Rab11a^+$ and $MMP7^+$ vesicles. This colocalization pattern was similar to that between Rab11a and MMP2, indicating that a fraction of MMP7 proteins transit through $Rab11a^+$ vesicles.

To definitively test whether $Rab11a^{null}$ blastocysts secreted less MMP7, we measured MMP7-specific enzymatic activities from supernatants of blastocyst culture medium, using a FRET-based enzyme kinetics assay. We seeded individual fertilized embryos, allowed them to hatch, and performed the assays on single hatched embryos. The genotype of each individual embryo was determined by PCR after the assay. In contrast to wild-type and heterozygous embryos that demonstrated a steady increase of substrate fluorescence correlating with MMP7 enzymatic cleavage activities, $Rab11a^{null}$ embryos had virtually no secreted MMP7 enzyme activity in the media (Fig. 5, *D* and *E*). These data supported the hypothesis that MMP7 secretion was impaired in $Rab11a^{null}$ blastocysts.

Defective Matrix Degradation by $Rab11a^{null}$ Blastocysts—Our data above indicated an intracellular association of MMP2 with $Rab11a^+$ vesicles (Fig. 3C). We then examined whether the same was true in mouse blastocysts. Costaining of MMP2 and Rab11a in wild-type blastocysts showed that a fraction of $MMP2^+$ vesicles were also positive for Rab11a, suggesting that a similar Rab11a-dependent MMP2 export mechanism may be employed in both MEFs and blastocysts (Fig. 6*A*).

Previous studies have demonstrated that the degradation of the extracellular matrix by blastocyst outgrowth could be used as an *in vitro* model for embryo implantation (55, 57). To directly assess the *in vivo* regulation of gelatinase (*e.g.* MMP2 and MMP9) secretion by Rab11a, we performed an *in vitro* matrix degradation assay using wild-type and null blastocysts. Blastocysts developed from fertilized eggs from $Rab11a^{+/-}$

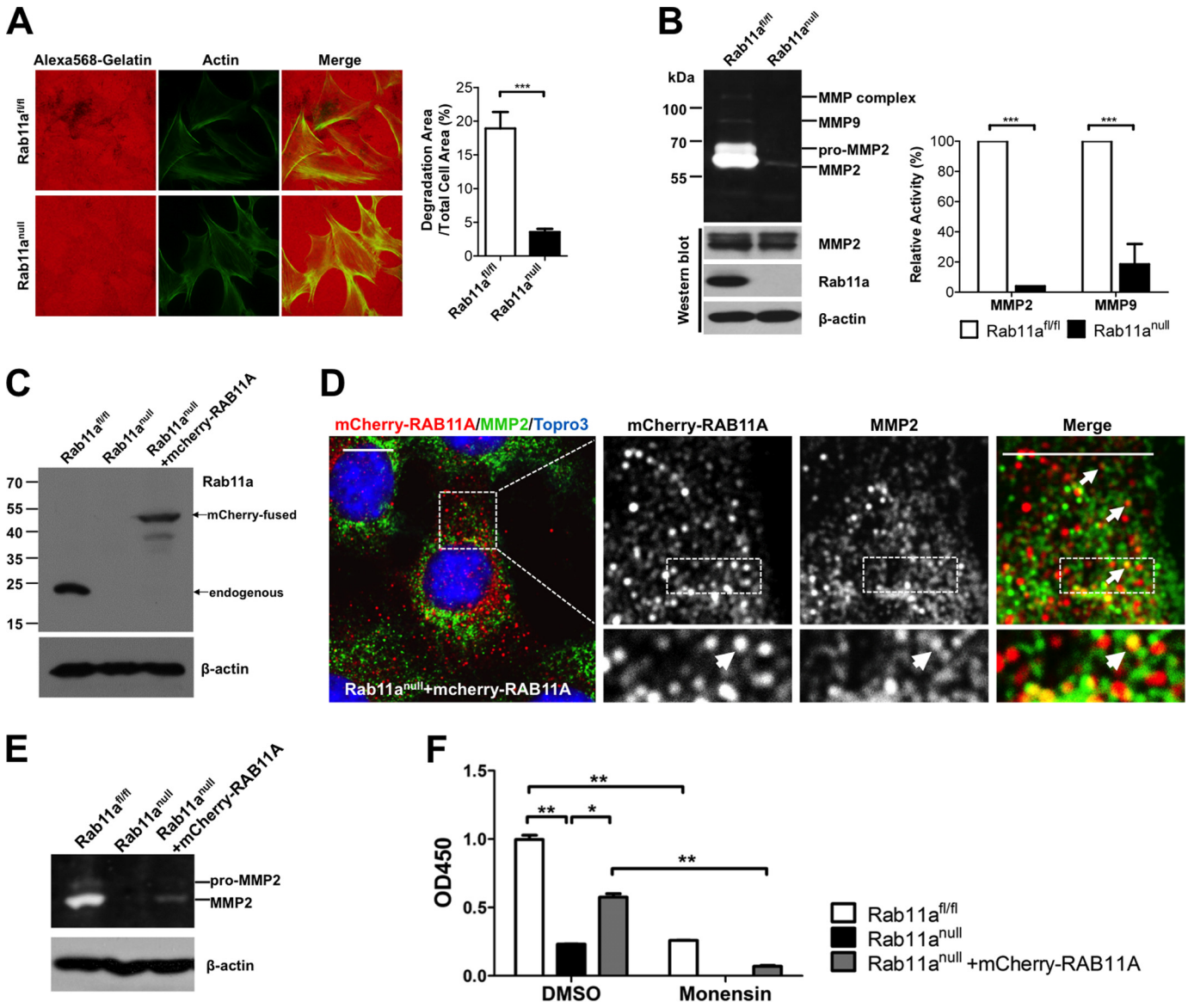

FIGURE 4. **Rab11a ablation impairs MMP2 secretion in MEFs.** *A*, extracellular matrix degradation assays showed reduced gelatin degradation by Rab11a^{null} MEFs (*bottom row*), compared with wild-type MEFs (*top row*). Degradation areas were quantified from three independent experiments. ***, $p < 0.001$. *B*, in-gel zymography assays showed reduced MMP2 and MMP9 secretion by Rab11a^{null} MEFs. Shown are quantified zymography measurements of MMP2 and MMP9 from three independent experiments. ***, $p < 0.001$. *C*, Western blot analyses detected the expression of exogenous mCherry-RAB11A in stably infected Rab11a^{null} MEFs. *D*, confocal immunofluorescent staining of mCherry-RAB11A rescued *Rab11a^{null}* MEFs. Colocalization of some endogenous MMP2 vesicles (*green*) with mCherry-RAB11A (*red*) was detected (*arrows*). *Scale bars* = 10 μm. *E*, zymography assays using the mCherry-RAB11A rescued Rab11a^{null} MEFs showed partially restored MMP2 activities. *F*, MMP2-specific ELISA showed a decreased MMP2 secretion by Rab11a^{null} MEFs compared with wild-type MEFs. Monensin also inhibited MMP2 secretion in wild-type MEFs. mCherry-RAB11A-rescued Rab11a^{null} MEFs showed a partial restoration of MMP2 secretion, which remained sensitive to monensin blockage. Data represent two independent experiments. *, $p < 0.05$; **, $p < 0.01$. *DMSO*, dimethyl sulfoxide.

mating were seeded on gelatin 568/collagen I-coated coverslips. After 2–3 days of culture, significant degradation of the matrix was observed for Rab11a^{+} wild-type blastocysts, illustrated by the loss of gelatin 568 (red) fluorescent signals (Fig. 6, *B*, *left column*, and *C*, *top row*). In contrast, Rab11a^{null} blastocysts showed significantly weakened degradation by ~78.5% (Fig. 6, *B*, *right column*, *C*, *bottom row*, and *D*), strongly supporting the hypothesis that Rab11a^{null} blastocysts had a poor capacity for secreting extracellular matrix-degrading MMPs.

In aggregates, our data suggested that the secretion of MMPs, a group of soluble biosynthetic cargo, was sensitively dependent on the function of Rab11a in at least two loss-of-function genetic settings, namely the trophoblasts and fetal fibroblasts.

DISCUSSION

In this study, we globally ablated Rab11a in mice and observed an embryonic lethal phenotype. Further embryonic culture and inducible Rab11a deletion experiments suggested that the lethality likely occurred at or shortly after the implantation stage. Different Rab small GTPases regulate distinct events of intracellular membrane trafficking. Global ablation of several other individual Rab regulators of the late endosome (Rab7), lysosome (Rab27), and post-Golgi exocytic vesicular

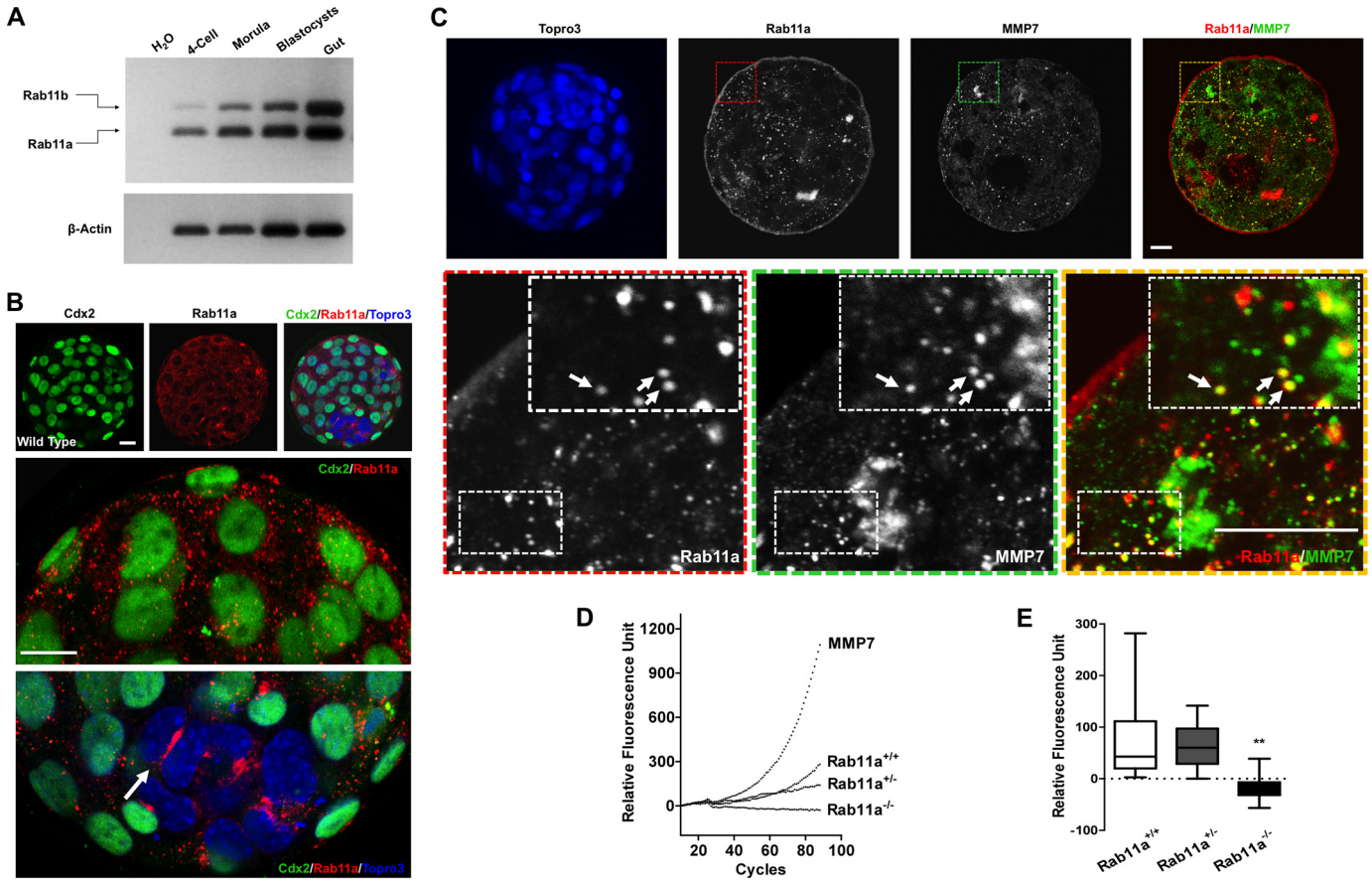

FIGURE 5. **Rab11a deficiency impairs MMP7 secretion in blastocysts.** *A*, RT-PCR detected Rab11a and Rab11b in embryos at the four-cell, morula, and blastocyst stages. Mouse gut total RNAs served as a control. *B*, immunofluorescent staining for Cdx2 (*green*) and Rab11a (*red*) in blastocysts. Both trophectoderm cells ($Cdx2^+$) and the inner cell mass ($Cdx2^-$) express Rab11a. The *arrow* points to intense Rab11a signals at a cleavage furrow within the inner cell mass. *Scale bars* = 20 μm. *C*, immunofluorescent staining for MMP7 (*green*) and Rab11a (*red*) in wild-type embryos. *Scale bars* = 10 μm. Some $MMP7^+$ vesicles were positive for Rab11a (*arrows*). *D*, MMP7 enzymatic kinetics were measured from the medium of cultured $Rab11a^{+/+}$, $Rab11a^{+/-}$, and $Rab11a^{-/-}$ hatching blastocysts. Bovine serum served as positive control. Values obtained from blank M16 medium were subtracted from all experimental values. *E*, accumulative MMP7 enzyme activities were averaged from the entire measuring duration. **, $p < 0.01$.

compartment (Rab8a and Rab8b) in mice did not prevent embryonic implantation (58–62). Our data suggest that Rab11a-mediated vesicular transport may be crucial for the very early stages of blastocyst development or invasion of the uterus. By analyzing a number of known and new cargos in $Rab11a^{null}$ blastocysts and fetal fibroblasts, we provided evidence for the involvement of Rab11a in the control of the secretion of a group of soluble MMPs in these physiological contexts.

When newly synthesized cargo proteins are transported to the TGN, sorting receptors are recruited to recognize sorting signal and segregate cargo into various vesicular carriers. In general, integral membrane cargos contain sorting signals at their cytosolic domains, associate with lipid rafts, or interact with lectins via glycan moieties further recognized by adaptors, v-SNAREs, and Rabs (1). VSVG is a well characterized transmembrane biosynthetic cargo that is targeted to the basolateral plasma membrane via its tyrosine-based sorting motif (63). Previous studies have illustrated that VSVG traffics to the cell surface through Rab11-positive recycling endosome compartments (8, 44). Gravotta *et al.* (63) have further demonstrated that delivery of VSVG through the recycling endosome is dependent on an epithelium-specific adaptor protein 1B subunit, μ1B. Additional studies have reported that VSVG could be sorted onto the basolateral surface in the context of μ1B knockdown, probably via alternative AP3 or AP4 adaptor complexes (45, 46, 63). Our observation that VSVG was positively targeted to the plasma membrane in $Rab11a^{null}$ MEFs supported the presence of alternative routes in membrane trafficking of newly synthetic VSVG. In terms of TfR, we clearly identified a reduced recycling in $Rab11a^{null}$ MEFs. However, despite the slow recycling, most receptors were eventually returned to the plasma membrane, suggesting that loss of Rab11a did not totally prevent the recycling process in fibroblasts. In light of these TfR results, we speculate that the membrane targeting efficiency of VSVG might also be reduced in $Rab11a^{null}$ MEFs. At this moment, we have not formally determined whether there was a reduction in the speed of VSVG export in $Rab11a^{null}$ MEFs.

In contrast to membrane-associated cargos, soluble cargos do not possess classic sorting motifs at their C terminus recognized by cytoplasmic adaptors. Therefore, most soluble cargos probably require special receptors to communicate with the cytosolic sorting machinery. For example, soluble lysosomal enzymes are segregated in the TGN by binding to the mannose 6-phosphate receptor for delivery to endosomes (64). The type I transmembrane protein Sortilin serves as a sorting receptor for soluble interferon γ secretion (65). The genetic deletion of

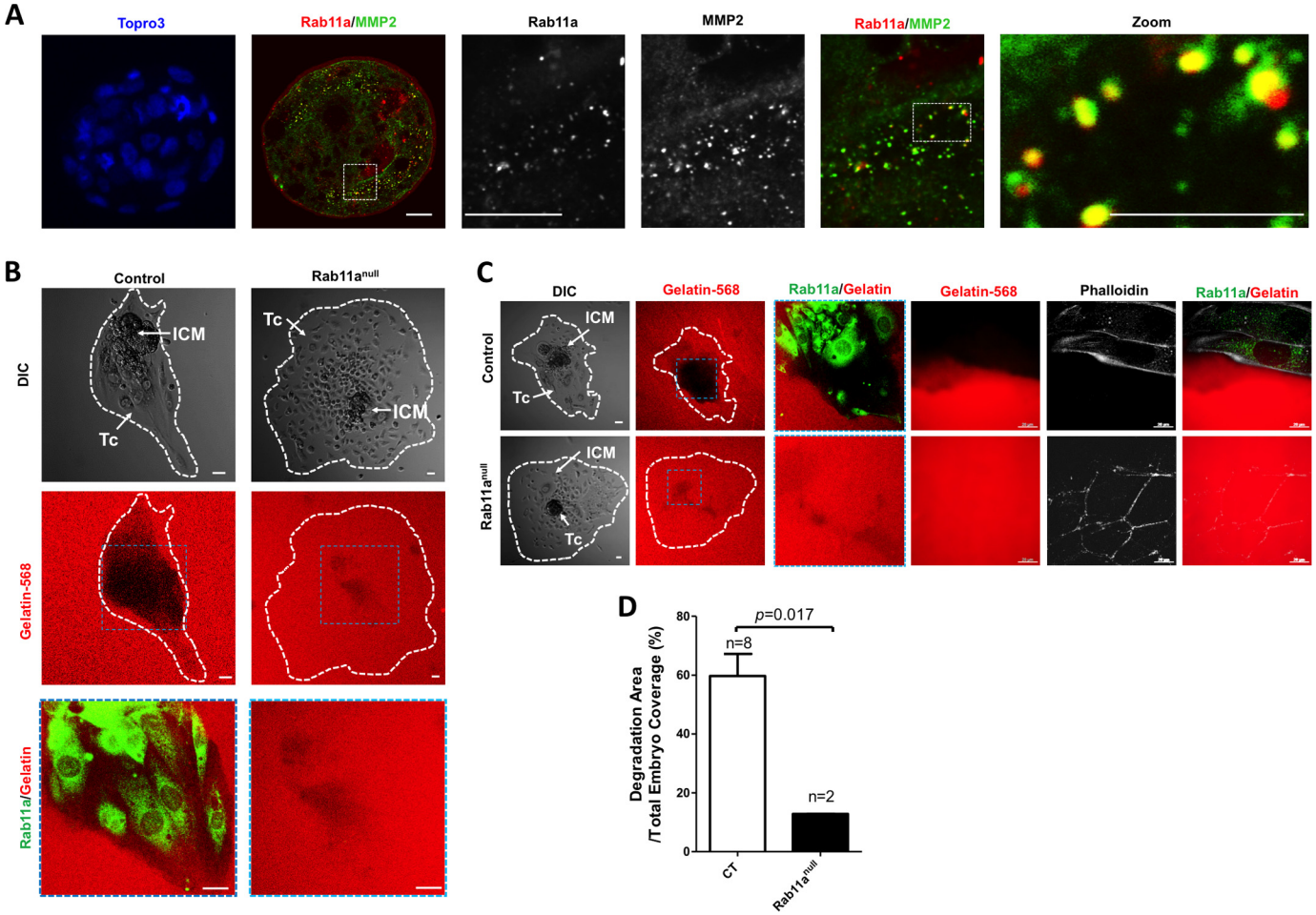

FIGURE 6. **Impaired gelatin degradation by Rab11a^{null} blastocysts.** *A*, confocal immunofluorescent staining on wild-type blastocysts showed colocalization between MMP2^{+} vesicles (*green*) and Rab11a (*red*). *Scale bars* = 10 μm. *B* and *C*, individual blastocysts (hatched) were seeded on chamber slides precoated with gelatin 568 (*red*). Extracellular matrix degradation activities, indicated by the loss of red fluorescent signals, by individual blastocysts were measured 3 days after embryo seeding. Rab11a staining (*green*) was used to identify null embryos. The leading edges of the embryo *C* were outlined by phalloidin 350 staining. *Scale bars* = 20 μm. *DIC*, differential interference contrast. *D*, the percentage of degradation areas were quantified and compared between wild-type and Rab11a^{null} blastocysts. *Tc*, trophoblastic cells; *ICM*, inner cell mass.

Sortilin caused a blockage of interferon γ in the Golgi complex. To date, the sorting receptor(s) for MMPs remain to be defined. Our data do suggest that the secretion of soluble MMPs is a regulated process because only a small fraction of MMP2 proteins is observed in TGN or post-Golgi vesicles compared with the large majority residing in the ER. Within the small fraction of vesicular MMPs, some MMP2^{+} or MMP7^{+} vesicles are clearly positive for Rab11a in both mouse blastocysts and MEFs. A lack of Rab11a vesicles in mouse blastocysts or MEFs dramatically reduced the secretion of multiple MMPs. Because we observed a marked Golgi accumulation of MMPs in the absence of Rab11a, we speculate that Rab11a probably acts to facilitate MMP transport from the TGN to post-Golgi vesicles. A recent study has demonstrated that tetraspanin protein family members modulate MT1-MMP intracellular trafficking via interaction with the hemopexin domain of MT1-MMP (66). Of note, soluble MMP2 and MMP9 also possess similar domains. Whether tetraspanin proteins also bind soluble MMPs to facilitate their export, and whether these same proteins bridge Rab11a and MMPs, are important questions for future exploration.

In light of previous reports that Rab11 mediates the secretion of soluble cytokines, interleukin 10, and interferon γ, in macrophages and natural killer cells (67, 68), it is not entirely surprising that Rab11a controls soluble MMP secretion in mouse trophoblasts and fetal fibroblasts. Both cell types engage in active matrix degradation and migration. The fact that Rab11a deficiency also impaired an artificial biosynthetic soluble cargo, SEAP, suggests that this Rab11a vesicular compartment might have a broader control of soluble cargos. Rescuing Rab11a^{null} MEFs with a human RAB11A partially restored MMP2 secretion, which remained sensitive to a recycling traffic inhibitor, strongly supporting the notion that the export of MMPs is crucially controlled by the Rab11a compartment, which intersects MMP vesicular trafficking in both mouse blastocyst and MEFs.

When fertilized, mouse oocytes undergo rapid cell division, forming embryos of two-cell, four-cell, morula, and blastocyst stages. The blastocyst possesses an outer trophectoderm and inner cell mass and forms a typical blastocoel (69). The subsequent expansion of the blastocyst increases the cavity pressure and facilitates the breakthrough of the zona pellucida by a group of "zona breaker" trophoblast cells and the escape of the

blastocyst. This hatching process renders the embryo competent for implantation, which involves the intricate succession and coordination of reciprocal interactions between proteins in the blastocyst and receptive uterus (51, 70, 71). During fetal implantation, trophoblasts secrete MMPs at the implantation site to invade the uterus, a process confirmed by *in vitro* studies to be essential for successful implantation and placentation (51). Our MMP7 enzymatic kinetics and *in vitro* matrix degradation assays using single blastocysts showed that Rab11a^{null} embryos displayed poor degrading activity toward the extracellular gelatin matrix with virtually no secreted MMP7 activity. The impact of Rab11a deficiency on MMP2 and MMP9 secretion in Rab11a^{null} blastocysts and MEFs collectively suggested that Rab11a vesicles might control the secretion of a group of MMPs rather than a single MMP protein. This notion was consistent with the fact that Rab11a^{null} embryos showed a more severe (lethal) phenotype than mice lacking single MMP genes (72, 73). The loss of Rab11a might have caused a combined impairment of the secretion of multiple MMPs, and, possibly, other molecules, in the implanting blastocysts. Overall, the involvement of Rab11a in secreting MMPs in different cell types identified MMPs as a prominent group of cargos depending on Rab11a vesicular transport.

Although our analyses focused on soluble MMP secretion from blastocysts and MEFs, they did not exclude the possibility that sorting or secretion of additional cargos might also be impaired in these systems. Nevertheless, this study, in our view, did bring fresh insights into the critical dependence of certain soluble biosynthetic cargos on Rab11a vesicles.

In contrast to the clear impact on MMP secretion, our study also indicated the cell type-dependent traffic of selective cargos by Rab11a. In the *Drosophila* egg chamber, Rab11 vesicles transport E-cadherin to maintain junctions between germ cells and niche cap cells (11, 12), whereas we observed morphologically normal blastocysts with E-cadherin localized to cell junctions in polarized Rab11a^{null} blastocysts. The fact that Rab11a^{null} blastocysts developed into the hatching stage strongly hinted at the normal formation of epithelial cell junctions in the embryo because E-cadherin mistrafficking would inevitably prevent embryonic compaction and morula formation, thus being lethal, as demonstrated by genetic studies (48, 49). In fact, Rab11a has been described as a bystander in basolateral recycling in polarized MDCK cells (74), suggesting that Rab11a-mediated E-cadherin trafficking may be cell type-dependent. Alternatively, Rab11b, whose expression was also detected from four-cell-stage embryos and onward, is involved in both apical and basolateral trafficking (75, 76). Therefore, Rab11b might potentially compensate Rab11a in trafficking E-cadherin in the mouse embryo. Such a compensatory mechanism in trafficking E-cadherin would be in accordance with the fact that the fly genome has only a single Rab11 gene. Nevertheless, Rab11b clearly failed to fully compensate for the loss of Rab11a during mouse embryogenesis, arguing that the traffic of certain cargos, such as MMPs, might be more sensitively dependent on Rab11a. In summary, we conclude that mouse Rab11a contributes to early fetal development and controls the secretion of soluble MMPs in both blastocysts and embryonic fibroblasts.

Acknowledgments—We thank Edward Martinez for help with some mouse experiments and Dr. Nihal Altan-Bonnet for some of the plasmids.

REFERENCES

1. Bard, F., and Malhotra, V. (2006) The formation of TGN-to-plasma-membrane transport carriers. *Annu. Rev. Cell Dev. Biol.* **22,** 439–455
2. De Matteis, M. A., and Luini, A. (2008) Exiting the Golgi complex. *Nat. Rev. Mol. Cell Biol.* **9,** 273–284
3. Sorkin, A., and von Zastrow, M. (2009) Endocytosis and signalling: intertwining molecular networks. *Nat. Rev. Mol. Cell Biol.* **10,** 609–622
4. Stenmark, H. (2009) Rab GTPases as coordinators of vesicle traffic. *Nat. Rev. Mol. Cell Biol.* **10,** 513–525
5. Hutagalung, A. H., and Novick, P. J. (2011) Role of Rab GTPases in membrane traffic and cell physiology. *Physiol. Rev.* **91,** 119–149
6. Welz, T., Wellbourne-Wood, J., and Kerkhoff, E. (2014) Orchestration of cell surface proteins by Rab11. *Trends Cell Biol.* **24,** 407–415
7. Grant, B. D., and Donaldson, J. G. (2009) Pathways and mechanisms of endocytic recycling. *Nat. Rev. Mol. Cell Biol.* **10,** 597–608
8. Chen, W., Feng, Y., Chen, D., and Wandinger-Ness, A. (1998) Rab11 is required for trans-Golgi network-to-plasma membrane transport and a preferential target for GDP dissociation inhibitor. *Mol. Biol. Cell* **9,** 3241–3257
9. Mattila, P. E., Youker, R. T., Mo, D., Bruns, J. R., Cresawn, K. O., Hughey, R. P., Ihrke, G., and Weisz, O. A. (2012) Multiple biosynthetic trafficking routes for apically secreted proteins in MDCK cells. *Traffic* **13,** 433–442
10. Lock, J. G., and Stow, J. L. (2005) Rab11 in recycling endosomes regulates the sorting and basolateral transport of E-cadherin. *Mol. Biol. Cell* **16,** 1744–1755
11. Bogard, N., Lan, L., Xu, J., and Cohen, R. S. (2007) Rab11 maintains connections between germline stem cells and niche cells in the *Drosophila* ovary. *Development* **134,** 3413–3418
12. Dollar, G., Struckhoff, E., Michaud, J., and Cohen, R. S. (2002) Rab11 polarization of the *Drosophila* oocyte: a novel link between membrane trafficking, microtubule organization, and oskar mRNA localization and translation. *Development* **129,** 517–526
13. Apodaca, G., Gallo, L. I., and Bryant, D. M. (2012) Role of membrane traffic in the generation of epithelial cell asymmetry. *Nat. Cell Biol.* **14,** 1235–1243
14. Goldenring, J. R., Smith, J., Vaughan, H. D., Cameron, P., Hawkins, W., and Navarre, J. (1996) Rab11 is an apically located small GTP-binding protein in epithelial tissues. *Am. J. Physiol.* **270,** G515–G525
15. Gao, N., and Kaestner, K. H. (2010) Cdx2 regulates endo-lysosomal function and epithelial cell polarity. *Genes Dev.* **24,** 1295–1305
16. Nakatsu, Y., Ma, X., Seki, F., Suzuki, T., Iwasaki, M., Yanagi, Y., Komase, K., and Takeda, M. (2013) Intracellular transport of the measles virus ribonucleoprotein complex is mediated by Rab11A-positive recycling endosomes and drives virus release from the apical membrane of polarized epithelial cells. *J. Virol.* **87,** 4683–4693
17. Eisfeld, A. J., Kawakami, E., Watanabe, T., Neumann, G., and Kawaoka, Y. (2011) RAB11A is essential for transport of the influenza virus genome to the plasma membrane. *J. Virol.* **85,** 6117–6126
18. Chambers, R., and Takimoto, T. (2010) Trafficking of Sendai virus nucleocapsids is mediated by intracellular vesicles. *PloS ONE* **5,** e10994
19. Vu, T. H., and Werb, Z. (2000) Matrix metalloproteinases: effectors of development and normal physiology. *Genes Dev.* **14,** 2123–2133
20. Parks, W. C., Wilson, C. L., and López-Boado, Y. S. (2004) Matrix metalloproteinases as modulators of inflammation and innate immunity. *Nat. Rev. Immunol.* **4,** 617–629
21. Page-McCaw, A., Ewald, A. J., and Werb, Z. (2007) Matrix metalloproteinases and the regulation of tissue remodelling. *Nat. Rev. Mol. Cell Biol.* **8,** 221–233
22. Visse, R., and Nagase, H. (2003) Matrix metalloproteinases and tissue inhibitors of metalloproteinases: structure, function, and biochemistry. *Circ. Res.* **92,** 827–839
23. Staun-Ram, E., Goldman, S., Gabarin, D., and Shalev, E. (2004) Expression

and importance of matrix metalloproteinase 2 and 9 (MMP-2 and -9) in human trophoblast invasion. *Reproductive Biology and Endocrinology* **2,** 59
24. Stanton, J. L., and Green, D. P. (2002) A set of 1542 mouse blastocyst and pre-blastocyst genes with well-matched human homologues. *Mol. Hum. Reprod.* **8,** 149–166
25. Poincloux, R., Lizárraga, F., and Chavrier, P. (2009) Matrix invasion by tumour cells: a focus on MT1-MMP trafficking to invadopodia. *J. Cell Sci.* **122,** 3015–3024
26. Sbai, O., Ferhat, L., Bernard, A., Gueye, Y., Ould-Yahoui, A., Thiolloy, S., Charrat, E., Charton, G., Tremblay, E., Risso, J. J., Chauvin, J. P., Arsanto, J. P., Rivera, S., and Khrestchatisky, M. (2008) Vesicular trafficking and secretion of matrix metalloproteinases-2, -9 and tissue inhibitor of metalloproteinases-1 in neuronal cells. *Mol. Cell. Neurosci.* **39,** 549–568
27. Hanania, R., Sun, H. S., Xu, K., Pustylnik, S., Jeganathan, S., and Harrison, R. E. (2012) Classically activated macrophages use stable microtubules for matrix metalloproteinase-9 (MMP-9) secretion. *J. Biol. Chem.* **287,** 8468–8483
28. Lapierre, L. A., Kumar, R., Hales, C. M., Navarre, J., Bhartur, S. G., Burnette, J. O., Provance, D. W., Jr., Mercer, J. A., Bähler, M., and Goldenring, J. R. (2001) Myosin vb is associated with plasma membrane recycling systems. *Mol. Biol. Cell* **12,** 1843–1857
29. Kean, M. J., Williams, K. C., Skalski, M., Myers, D., Burtnik, A., Foster, D., and Coppolino, M. G. (2009) VAMP3, syntaxin-13 and SNAP23 are involved in secretion of matrix metalloproteinases, degradation of the extracellular matrix and cell invasion. *J. Cell Sci.* **122,** 4089–4098
30. Gorodeski, G. I. (2007) Estrogen decrease in tight junctional resistance involves matrix-metalloproteinase-7-mediated remodeling of occludin. *Endocrinology* **148,** 218–231
31. Steffen, A., Le Dez, G., Poincloux, R., Recchi, C., Nassoy, P., Rottner, K., Galli, T., and Chavrier, P. (2008) MT1-MMP-dependent invasion is regulated by TI-VAMP/VAMP7. *Curr. Biol.* **18,** 926–931
32. Wiesner, C., El Azzouzi, K., and Linder, S. (2013) A specific subset of RabGTPases controls cell surface exposure of MT1-MMP, extracellular matrix degradation and three-dimensional invasion of macrophages. *J. Cell Sci.* **126,** 2820–2833
33. Jacob, A., Jing, J., Lee, J., Schedin, P., Gilbert, S. M., Peden, A. A., Junutula, J. R., and Prekeris, R. (2013) Rab40b regulates trafficking of MMP2 and MMP9 during invadopodia formation and invasion of breast cancer cells. *J. Cell Sci.* **126,** 4647–4658
34. Liu, P., Jenkins, N. A., and Copeland, N. G. (2003) A highly efficient recombineering-based method for generating conditional knockout mutations. *Genome Res.* **13,** 476–484
35. Yu, S., Nie, Y., Knowles, B., Sakamori, R., Stypulkowski, E., Patel, C., Das, S., Douard, V., Ferraris, R. P., Bonder, E. M., Goldenring, J. R., Ip, Y. T., and Gao, N. (2014) TLR sorting by Rab11 endosomes maintains intestinal epithelial-microbial homeostasis. *EMBO J.* **33,** 1882–1895
36. Rodríguez, C. I., Buchholz, F., Galloway, J., Sequerra, R., Kasper, J., Ayala, R., Stewart, A. F., and Dymecki, S. M. (2000) High-efficiency deleter mice show that FLPe is an alternative to Cre-loxP. *Nat. Genet.* **25,** 139–140
37. Lakso, M., Pichel, J. G., Gorman, J. R., Sauer, B., Okamoto, Y., Lee, E., Alt, F. W., and Westphal, H. (1996) Efficient *in vivo* manipulation of mouse genomic sequences at the zygote stage. *Proc. Natl. Acad. Sci. U.S.A.* **93,** 5860–5865
38. Ventura, A., Kirsch, D. G., McLaughlin, M. E., Tuveson, D. A., Grimm, J., Lintault, L., Newman, J., Reczek, E. E., Weissleder, R., and Jacks, T. (2007) Restoration of p53 function leads to tumour regression *in vivo*. *Nature* **445,** 661–665
39. Zlatkine, P., Mehul, B., and Magee, A. I. (1997) Retargeting of cytosolic proteins to the plasma membrane by the Lck protein tyrosine kinase dual acylation motif. *J. Cell Sci.* **110**, 673–679
40. Liu, J., Yue, P., Artym, V. V., Mueller, S. C., and Guo, W. (2009) The role of the exocyst in matrix metalloproteinase secretion and actin dynamics during tumor cell invadopodia formation. *Mol. Biol. Cell* **20,** 3763–3771
41. Sakamori, R., Yu, S., Zhang, X., Hoffman, A., Sun, J., Das, S., Vedula, P., Li, G., Fu, J., Walker, F., Yang, C. S., Yi, Z., Hsu, W., Yu, D. H., Shen, L., Rodriguez, A. J., Taketo, M. M., Bonder, E. M., Verzi, M. P., and Gao, N. (2014) CDC42 Inhibition suppresses progression of incipient intestinal tumors. *Cancer Res.* **74,** 5480–5492
42. Ullrich, O., Reinsch, S., Urbé, S., Zerial, M., and Parton, R. G. (1996) Rab11 regulates recycling through the pericentriolar recycling endosome. *J. Cell Biol.* **135,** 913–924
43. Ren, M., Xu, G., Zeng, J., De Lemos-Chiarandini, C., Adesnik, M., and Sabatini, D. D. (1998) Hydrolysis of GTP on rab11 is required for the direct delivery of transferrin from the pericentriolar recycling compartment to the cell surface but not from sorting endosomes. *Proc. Natl. Acad. Sci. U.S.A.* **95,** 6187–6192
44. Ang, A. L., Taguchi, T., Francis, S., Fölsch, H., Murrells, L. J., Pypaert, M., Warren, G., and Mellman, I. (2004) Recycling endosomes can serve as intermediates during transport from the Golgi to the plasma membrane of MDCK cells. *J. Cell Biol.* **167,** 531–543
45. Fields, I. C., Shteyn, E., Pypaert, M., Proux-Gillardeaux, V., Kang, R. S., Galli, T., and Fölsch, H. (2007) v-SNARE cellubrevin is required for basolateral sorting of AP-1B-dependent cargo in polarized epithelial cells. *J. Cell Biol.* **177,** 477–488
46. Nishimura, N., Plutner, H., Hahn, K., and Balch, W. E. (2002) The δ subunit of AP-3 is required for efficient transport of VSV-G from the trans-Golgi network to the cell surface. *Proc. Natl. Acad. Sci. U.S.A.* **99,** 6755–6760
47. Solis, G. P., Hülsbusch, N., Radon, Y., Katanaev, V. L., Plattner, H., and Stuermer, C. A. (2013) Reggies/flotillins interact with Rab11a and SNX4 at the tubulovesicular recycling compartment and function in transferrin receptor and E-cadherin trafficking. *Mol. Biol. Cell* **24,** 2689–2702
48. Larue, L., Ohsugi, M., Hirchenhain, J., and Kemler, R. (1994) E-cadherin null mutant embryos fail to form a trophectoderm epithelium. *Proc. Natl. Acad. Sci. U.S.A.* **91,** 8263–8267
49. Riethmacher, D., Brinkmann, V., and Birchmeier, C. (1995) A targeted mutation in the mouse E-cadherin gene results in defective preimplantation development. *Proc. Natl. Acad. Sci. U.S.A.* **92,** 855–859
50. Berger, J., Hauber, J., Hauber, R., Geiger, R., and Cullen, B. R. (1988) Secreted placental alkaline phosphatase: a powerful new quantitative indicator of gene expression in eukaryotic cells. *Gene* **66,** 1–10
51. van Mourik, M. S., Macklon, N. S., and Heijnen, C. J. (2009) Embryonic implantation: cytokines, adhesion molecules, and immune cells in establishing an implantation environment. *J. Leukocyte Biol.* **85,** 4–19
52. Solnica-Krezel, L., and Sepich, D. S. (2012) Gastrulation: making and shaping germ layers. *Annu. Rev. Cell Dev. Biol.* **28,** 687–717
53. Xia, S., Kjaer, S., Zheng, K., Hu, P. S., Bai, L., Jia, J. Y., Rigler, R., Pramanik, A., Xu, T., Hökfelt, T., and Xu, Z. Q. (2004) Visualization of a functionally enhanced GFP-tagged galanin R2 receptor in PC12 cells: constitutive and ligand-induced internalization. *Proc. Natl. Acad. Sci. U.S.A.* **101,** 15207–15212
54. Baratti-Elbaz, C., Ghinea, N., Lahuna, O., Loosfelt, H., Pichon, C., and Milgrom, E. (1999) Internalization and recycling pathways of the thyrotropin receptor. *Mol. Endocrinol.* **13,** 1751–1765
55. Behrendtsen, O., Alexander, C. M., and Werb, Z. (1992) Metalloproteinases mediate extracellular matrix degradation by cells from mouse blastocyst outgrowths. *Development* **114,** 447–456
56. Staun-Ram, E., and Shalev, E. (2005) Human trophoblast function during the implantation process. *Reproductive Biology and Endocrinology* **3,** 56
57. Glass, R. H., Aggeler, J., Spindle, A., Pedersen, R. A., and Werb, Z. (1983) Degradation of extracellular matrix by mouse trophoblast outgrowths: a model for implantation. *J. Cell Biol.* **96,** 1108–1116
58. Sato, T., Mushiake, S., Kato, Y., Sato, K., Sato, M., Takeda, N., Ozono, K., Miki, K., Kubo, Y., Tsuji, A., Harada, R., and Harada, A. (2007) The Rab8 GTPase regulates apical protein localization in intestinal cells. *Nature* **448,** 366–369
59. Wilson, S. M., Yip, R., Swing, D. A., O'Sullivan, T. N., Zhang, Y., Novak, E. K., Swank, R. T., Russell, L. B., Copeland, N. G., and Jenkins, N. A. (2000) A mutation in Rab27a causes the vesicle transport defects observed in ashen mice. *Proc. Natl. Acad. Sci. U.S.A.* **97,** 7933–7938
60. Tolmachova, T., Abrink, M., Futter, C. E., Authi, K. S., and Seabra, M. C. (2007) Rab27b regulates number and secretion of platelet dense granules. *Proc. Natl. Acad. Sci. U.S.A.* **104,** 5872–5877
61. Kawamura, N., Sun-Wada, G. H., Aoyama, M., Harada, A., Takasuga, S., Sasaki, T., and Wada, Y. (2012) Delivery of endosomes to lysosomes via

microautophagy in the visceral endoderm of mouse embryos. *Nat. Commun.* **3,** 1071
62. Sato, T., Iwano, T., Kunii, M., Matsuda, S., Mizuguchi, R., Jung, Y., Hagiwara, H., Yoshihara, Y., Yuzaki, M., Harada, R., and Harada, A. (2014) Rab8a and Rab8b are essential for several apical transport pathways but insufficient for ciliogenesis. *J. Cell Sci.* **127,** 422–431
63. Gravotta, D., Deora, A., Perret, E., Oyanadel, C., Soza, A., Schreiner, R., Gonzalez, A., and Rodriguez-Boulan, E. (2007) AP1B sorts basolateral proteins in recycling and biosynthetic routes of MDCK cells. *Proc. Natl. Acad. Sci. U.S.A.* **104,** 1564–1569
64. Ghosh, P., Dahms, N. M., and Kornfeld, S. (2003) Mannose 6-phosphate receptors: new twists in the tale. *Nat. Rev. Mol. Cell Biol.* **4,** 202–212
65. Herda, S., Raczkowski, F., Mittrücker, H. W., Willimsky, G., Gerlach, K., Kühl, A. A., Breiderhoff, T., Willnow, T. E., Dörken, B., Höpken, U. E., and Rehm, A. (2012) The sorting receptor Sortilin exhibits a dual function in exocytic trafficking of interferon-γ and granzyme A in T cells. *Immunity* **37,** 854–866
66. Schröder, H. M., Hoffmann, S. C., Hecker, M., Korff, T., and Ludwig, T. (2013) The tetraspanin network modulates MT1-MMP cell surface trafficking. *Int. J. Biochem. Cell Biol.* **45,** 1133–1144
67. Reefman, E., Kay, J. G., Wood, S. M., Offenhäuser, C., Brown, D. L., Roy, S., Stanley, A. C., Low, P. C., Manderson, A. P., and Stow, J. L. (2010) Cytokine secretion is distinct from secretion of cytotoxic granules in NK cells. *J. Immunol.* **184,** 4852–4862
68. Stanley, A. C., Lieu, Z. Z., Wall, A. A., Venturato, J., Khromykh, T., Hamilton, N. A., Gleeson, P. A., and Stow, J. L. (2012) Recycling endosome-dependent and -independent mechanisms for IL-10 secretion in LPS-activated macrophages. *J. Leukocyte Biol.* **92,** 1227–1239
69. Wang, H., and Dey, S. K. (2006) Roadmap to embryo implantation: clues from mouse models. *Nat. Rev. Genet.* **7,** 185–199
70. Mor, G., Cardenas, I., Abrahams, V., and Guller, S. (2011) Inflammation and pregnancy: the role of the immune system at the implantation site. *Ann. N.Y. Acad. Sci.* **1221,** 80–87
71. Cha, J., Sun, X., and Dey, S. K. (2012) Mechanisms of implantation: strategies for successful pregnancy. *Nat. Med.* **18,** 1754–1767
72. Rudolph-Owen, L. A., Hulboy, D. L., Wilson, C. L., Mudgett, J., and Matrisian, L. M. (1997) Coordinate expression of matrix metalloproteinase family members in the uterus of normal, matrilysin-deficient, and stromelysin-1-deficient mice. *Endocrinology* **138,** 4902–4911
73. Itoh, T., Ikeda, T., Gomi, H., Nakao, S., Suzuki, T., and Itohara, S. (1997) Unaltered secretion of β-amyloid precursor protein in gelatinase A (matrix metalloproteinase 2)-deficient mice. *J. Biol. Chem.* **272,** 22389–22392
74. Wang, X., Kumar, R., Navarre, J., Casanova, J. E., and Goldenring, J. R. (2000) Regulation of vesicle trafficking in Madin-Darby canine kidney cells by Rab11a and Rab25. *J. Biol. Chem.* **275,** 29138–29146
75. Oehlke, O., Martin, H. W., Osterberg, N., and Roussa, E. (2011) Rab11b and its effector Rip11 regulate the acidosis-induced traffic of V-ATPase in salivary ducts. *J. Cell. Physiol.* **226,** 638–651
76. Silvis, M. R., Bertrand, C. A., Ameen, N., Golin-Bisello, F., Butterworth, M. B., Frizzell, R. A., and Bradbury, N. A. (2009) Rab11b regulates the apical recycling of the cystic fibrosis transmembrane conductance regulator in polarized intestinal epithelial cells. *Mol. Biol. Cell* **20,** 2337–2350